Available online at www.sciencedirect.com
ScienceDirect
Composite Structures 80 (2007) 361–372
COMPOSITE STRUCTURES
www.elsevier.com/locate/compstruct

2D modelling of a thin elasto-plastic interphase between two different materials: Plane strain case

Gennady Mishuris [a,*], Andreas Öchsner [b]

[a] Department of Mathematics, Rzeszów University of Technology, Rzeszów, Poland
[b] Centre for Mechanical Technology and Automation, Department of Mechanical Engineering, University of Aveiro, Aveiro, Portugal

Available online 27 June 2006

Abstract

A thin soft elasto-plastic interphase between two different media is under consideration. The intermediate layer is assumed to be of infinitesimal thickness and is modelled by non-linear transmission conditions which incorporate the elasto-plastic material behaviour of the layer. FEM analysis of a bimaterial structure with such an imperfect elasto-plastic interface shows the efficiency of the approach and illustrates some restrictions of its application.

Keywords: Elastic–plastic layer; Imperfect interface; Non-classical transmission conditions

1. Introduction

Thin interphases appearing in dissimilar bodies such as composite structures with adhesively bonded materials may significantly influence the whole spectrum of structural parameters: strength, dynamics, fracture, lifetime, and so on. Recently, significant efforts have been done to clarify various phenomena connected with the so-called elastic imperfect interface approach. It consists of replacing the real thin interphase between two different materials by an infinitesimal layer of zero thickness. This layer is then modelled by special transmission conditions which incorporate information about geometrical and mechanical properties of the thin interphase. At first, such proposed conditions were based on phenomenological approaches and have been sufficiently exploited (see [1–3] among others and the respective references). Later, various imperfect transmission conditions have been evaluated by asymptotic methods in [4–7] for different types of interfaces and materials. The accurate asymptotic behaviour of solutions of interface crack problems at the imperfect interface formulation has been investigated in [8–10] where it has been shown that the behaviour may be very complicated and essentially depending on the material and geometrical properties of the imperfect interfaces. Possible error estimates and ranges of the edge zone effects connected with utilisation of the imperfect models have been discussed in detail in [11,12] by FEM analysis. This short review shows that *elastic* imperfect interfaces have been intensively investigated in different directions.

However, thin elasto-plastic interfaces play even a more important role in real applications [13] and results which are obtained up to now are absolutely insufficient and are mainly concentrated on problems of thin plastic interphases between stiff adherends [14,15].

In the present work, imperfect transmission conditions for a soft elasto-plastic interphase are discussed. The interface is described by Hencky's deformation theory model. Only the main terms, i.e. zero-order expressions, of the asymptotic analysis are considered. Respective transmission conditions are naturally non-linear. Higher-order expressions can be later much easier constructed continuing the asymptotic procedure from the respective linear boundary problems. Numerical examples based on an accurate finite element simulations show the high efficiency

* Corresponding author. Tel.: +48 17 8651660; fax: +48 17 8543116.
E-mail address: miszuris@prz.rzeszow.pl (G. Mishuris).

0263-8223/$ - see front matter © 2006 Elsevier Ltd. All rights reserved.
doi:10.1016/j.compstruct.2006.05.017

of the approach, in spite of the fact that the deformation theory has its own strong restrictions.

2. Description of the thin elasto-plastic interface

Let us first consider only the elasto-plastic interphase and assume that its material behaviour can be modelled by Hencky's law [15,16]:

$$\varepsilon = \frac{1-2\nu}{E}\sigma, \quad \mathbf{D}_\varepsilon = \left(\phi + \frac{1}{2\mu}\right)\mathbf{D}_\sigma, \tag{1}$$

where ν is Poisson's ratio, μ and E are the shear and Young's modulae of the material in the elastic regime ($E = 2\mu(1+\nu)$). As usual, the first invariants of the strain and stress tensors are denoted by ε and σ. Furthermore, $\mathbf{D}_\varepsilon$ and $\mathbf{D}_\sigma$ are deviators of strain and stress, respectively, while $J_2(\boldsymbol{\varepsilon})$ and $J_2(\boldsymbol{\sigma})$ are their second invariants.

Function ϕ is known in Eq. (1) and it is assumed to depend only on the second invariant of the strain deviator [15]:

$$\phi = \phi(J_2(\boldsymbol{\varepsilon})), \tag{2}$$

where $\phi(t) = 0$ holds within the elastic region ($t \leqslant J_2(\boldsymbol{\varepsilon}_{cr})$, $\boldsymbol{\varepsilon}_{cr}$: initial yield strain tensor). It is well known that such a model appropriately describes only monotonic or nearly monotonic loading and, in fact, constitutes one of the non-linear elasticity models [15,17]. It can be rewritten in the elasticity-like form after transformations as

$$\sigma_{ij} = 2\tilde{\mu}\varepsilon_{ij} + \tilde{\lambda}\varepsilon\delta_{ij}, \quad i,j = 1,2,3, \tag{3}$$

where the generalised Lamé's coefficients are introduced by the following formulae:

$$\begin{aligned} \tilde{\mu}(\phi) &= \frac{1}{2}\left(\phi + \frac{1+\nu}{E}\right)^{-1}, \\ \tilde{\lambda}(\phi) &= \frac{1}{3}\left(\phi + \frac{1+\nu}{E}\right)^{-1}\left(\frac{3\nu}{1-2\nu} + \phi\frac{E}{1-2\nu}\right). \end{aligned} \tag{4}$$

Let us note that these coefficients simply coincide in the pure elastic regime ($\phi = 0$) with the respective elastic Lamé's parameters:

$$\tilde{\mu}(0) = \mu = \frac{E}{2(1+\nu)}, \quad \tilde{\lambda}(0) = \lambda = \frac{\nu E}{(1+\nu)(1-2\nu)}. \tag{5}$$

Using notations (4), the generalised Poisson's ratio can be defined in the following manner:

$$\tilde{\nu}(\phi) = \frac{\tilde{\lambda}(\phi)}{2(\tilde{\lambda}(\phi) + \tilde{\mu}(\phi))} = \frac{3\nu + \phi E}{3 + 2\phi E}. \tag{6}$$

In [18], new transmission conditions which describe the behaviour of a flat thin elasto-plastic interphase of constant thickness situated between two different materials have been evaluated by means of asymptotic techniques for a plane strain state. The only restriction to the model was that the adherends should be essentially stiffer than the interphase itself in all regimes (elastic or plastic ones). Assuming that the interface middle line is $y = 0$, the conditions take the following non-linear form [18]:

$$[\sigma_{xy}] = 0, \quad [\sigma_y] = 0, \tag{7}$$

$$F_x([u_x],[u_y]) = \sigma_{xy}, \quad F_y([u_x],[u_y]) = \sigma_y, \tag{8}$$

where $[f] = f(x,0+) - f(x,0-)$ is the jump of the function f along the infinitesimal interface $y = 0$. The functions on the left-hand sides of Eq. (8) are defined from the generalised Lamé's coefficients (20) given in Appendix, where the main ideas of the asymptotic analysis to evaluate the transmission conditions (7) and (8) are presented.

It is important to note that the transmission conditions (7) and (8) correspond to the main (zero-order) term of the asymptotic procedure. Next terms are also possible to construct. Moreover, they have to be found from solutions of the consequent *linear* boundary value problems for the corresponding degree of approximation. However, whereas it is also easy to prove the estimate of such an approach which is terminating the procedure at any step in the case of linear elasticity, the elasto-plastic interphase is a much more complicated problem due to the material non-linearity. In such cases, FEM analysis of modelling problems is the most effective way to check applicability of the transmission conditions and to discover its restrictions. This approach is utilised in the following.

3. Numerical examples

3.1. Metallic joints

The geometry of the sample and loading conditions are shown in Fig. 1. The real elasto-plastic behaviour of the aluminium alloy AlCuMg1 [19] is assigned to the metallic adherends which are adhesively bonded by the interface and it is assumed that both are identical with Young's modulae $E_\pm = 72{,}700$ MPa and Poisson's ratio $\nu_\pm = 0.34$. The geometrical dimensions are $L = 10$ mm, $H = 1$ mm and $2h = 0.01$ mm. As a result, the value of $\epsilon = 2h/H = 0.01$ can be considered as the small parameter.

Two different elasto-plastic interphases are considered: a linear hardening material model and an elastic-perfectly plastic material. Corresponding material parameters are described in Fig. 2(a). Namely, elastic parameters of the interphases are the same: $E = 813$ MPa, $\nu = 0.3$. In the

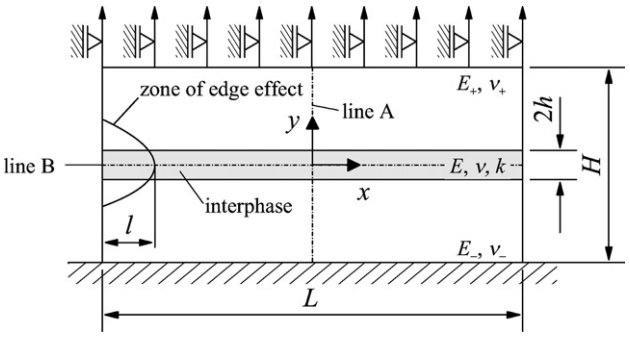

Fig. 1. Schematic representation of the problem, evaluation paths and boundary conditions of the investigated structure.

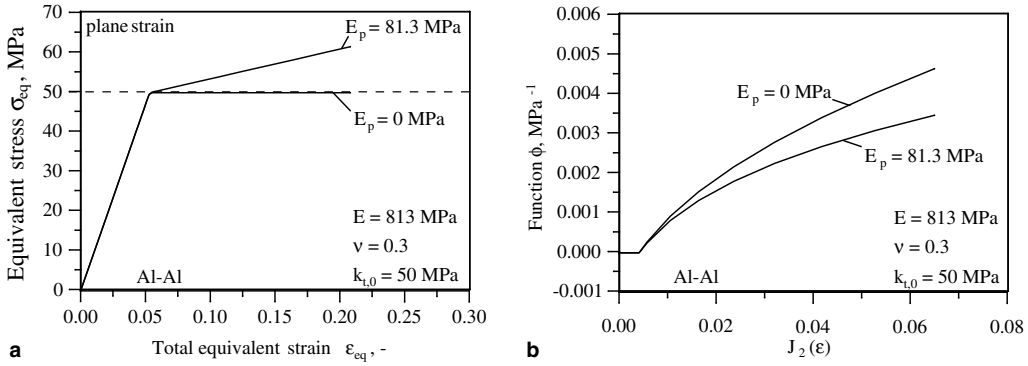

Fig. 2. (a) Material parameters of the interphase for metallic joints due to plastic flow theory and (b) function ϕ of Hencky's law.

plastic region which is appearing after reaching the Huber–Mises stress of value $k_{t,0} = 50$ MPa, the constant hardening modulus $E_p = 81.3$ MPa is prescribed for the hardening material and $k_t = k_{t,0}$ for the ideal plasticity case. Let us underline that all commercial FEM codes are based on the more general theory of plastic flow [15–17]. As it has been mentioned above, the results with these models (plastic flow and deformation theories) coincide only under monotonic or nearly monotonic loading. Because of this, only monotonic external loading is applied in the modelling approach (Dirichlet boundary condition at the top of the sample).

The respective functions ϕ involved in the deformation theory Eqs. (1) and (2) have been calculated by the given interphase properties of the flow theory [15,16] and its graphs are shown in Fig. 2(b). Furthermore, it was assumed in both cases that the elasto-plastic material is obeying the Huber–Mises yield criterion.

The commercial finite element code MSC.Marc is used for the simulation of the mechanical behaviour of the modelling thin intermediate elasto-plastic layer between two elastic adherends. The two-dimensional FE-mesh is built up of four-node, isoparametric elements with bilinear interpolation functions. In order to cover all possible edge effects [12] (cf. Fig. 1, left and right hand side of the interphase), a strong mesh refinement is performed in these regions, Fig. 3. The density of the elements along the interphase is shown in Fig. 4. Furthermore, the mesh is generated in such a way that it is possible to evaluate the displacements and stresses along the axes of geometrical symmetry, and along all the interfaces between the interphase elasto-plastic material and the adherends as well as along the lines parallel and perpendicular to the interfaces and lying within the interphase layer.

3.1.1. Elasto-plastic interphase with hardening law

3.1.1.1. Simple tensile loading. A simple monotonic tensile loading $(u_x(x, H/2) = 0, u_y(x, H/2) = v_y)$ is applied to the top of the bimaterial sample in the range from 0% to 0.6% of v_y/H in 100 incremental steps.

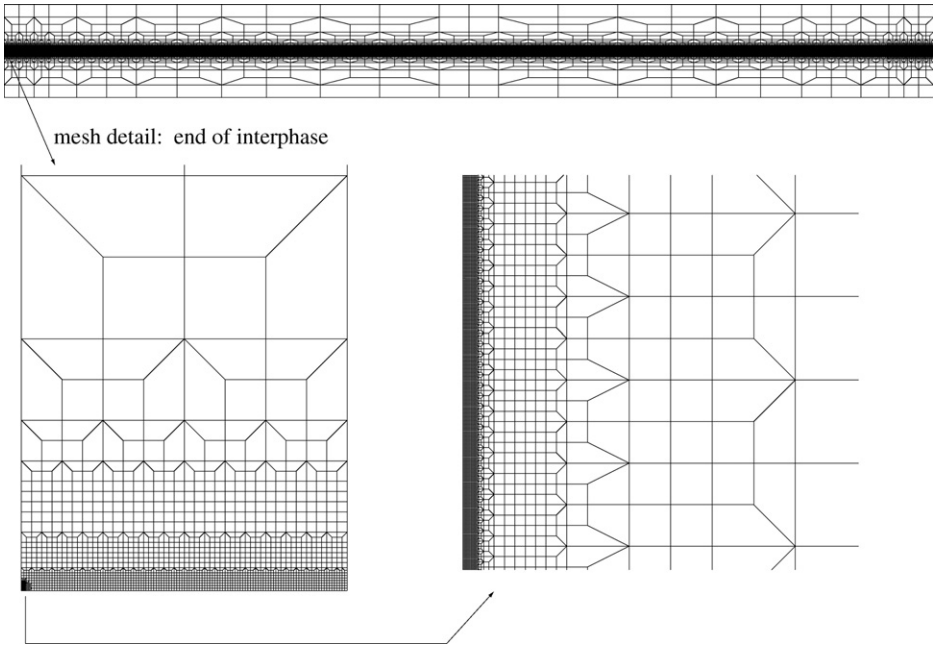

Fig. 3. Two-dimensional FE-mesh: strong mesh refinement in the investigated area.

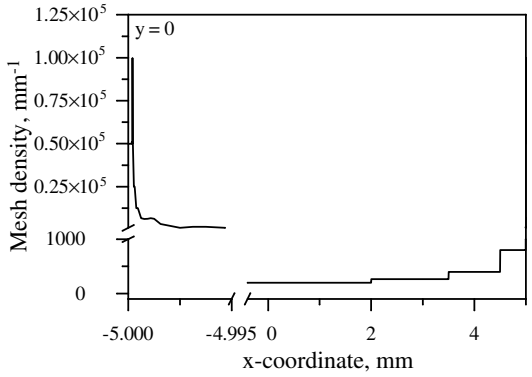

Fig. 4. Mesh density with reference to Fig. 1.

First of all, distributions of all displacements and stress components in direction perpendicular to the interface through the whole sample in its middle part (along the line A cf. Fig. 1) are shown in Figs. 5 and 6. Results presented in Figs. 5(a) and 6(a) correspond to the elastic regime while Figs. 5(b) and 6(b) are valid for the plastic deformation. As one can see, stresses within the interface are constant whereas the displacements are linear functions which completely coincides with the theoretical predictions. As a result, equivalent Huber–Mises stress and the equivalent plastic strain do not change within the interphase in direction perpendicular to its boundaries (for a fixed x). Its variation along the middle line of the elasto-plastic interphase is presented for several increments in Fig. 7.

Due to the symmetry of the loading and the sample geometry, two of the transmission conditions, i.e. $[\sigma_{xy}] = 0$ and $F_x([u_x],[u_y]) = \sigma_{xy}$, are satisfied identically because of $[u_x] = 0$ and $\sigma_{xy} = 0$ holds in this case. The remaining two conditions $[u_y] = 0$ and $F_y(0,[u_y]) = \sigma_y$ have to be verified. The first one is the same as in the case of the pure elastic imperfect interface [11], has the same order of accuracy as discovered in [11] and, because of this, it is of less interest in comparison with the second one.

In Fig. 8(a), comparisons of the left and right hand sides of the condition $F_y(0,[u_y]) = \sigma_y$ are presented. The traction is drawn by the solid line while the values of the left-hand side function in $(8)_2$ is depicted by circles in several points. The visible plastic zone appears in the middle of the interface at the 30th increment with a deformation ratio of $v_y/H = 0.18\%$. The accuracy of the evaluated transmission condition $(8)_2$ is in the same range as it has been checked for the pure elastic interface [11]. Moreover, the region where the transmission conditions are valid does not change practically regardless the interphase material is in the elastic or plastic region, Fig. 8(b). To highlight this fact, a magnification of the same functions as in Fig. 8(a) is presented in Fig. 8(b). A 1% accuracy criterion has been

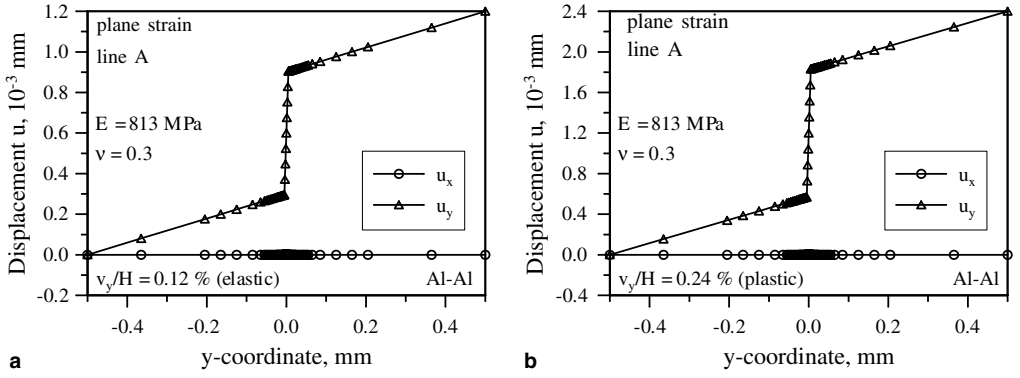

Fig. 5. Displacement distribution along line A (cf. Fig. 1) for an elastic and plastic stage inside the hardening interphase (simple tensile loading; aluminium adherends).

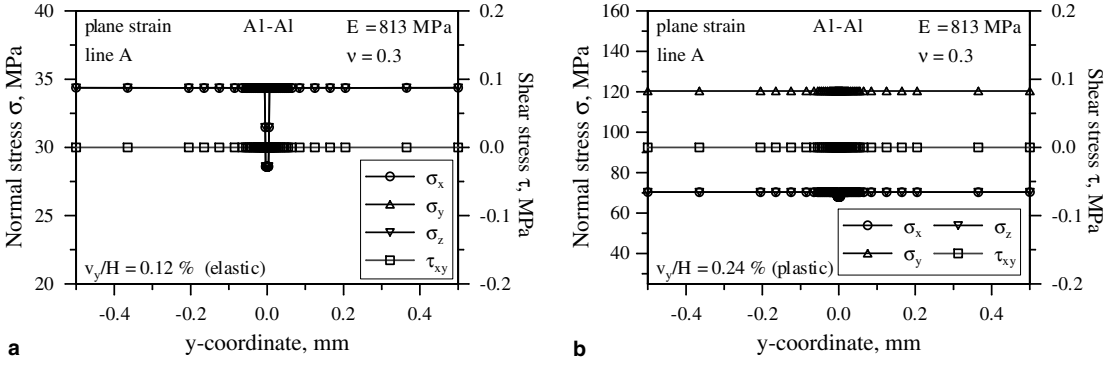

Fig. 6. Stress distribution along line A (cf. Fig. 1) for an elastic and plastic stage inside the hardening interphase (simple tensile loading; aluminium adherends).

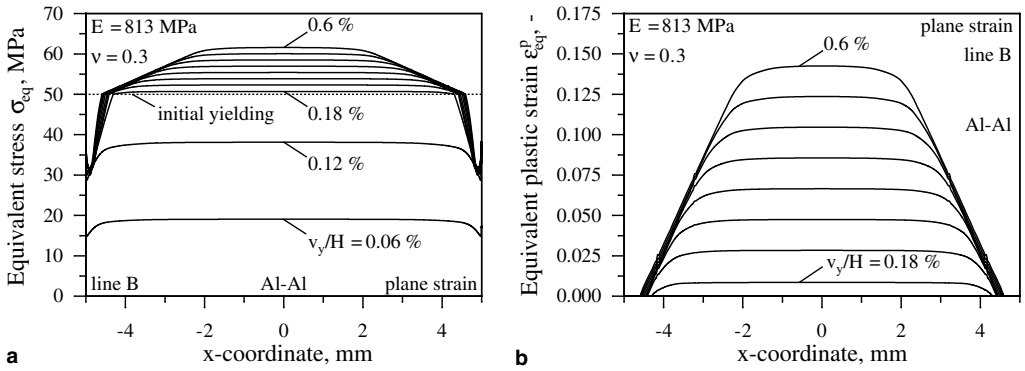

Fig. 7. Distribution of equivalent stress and strain along line B (cf. Fig. 1) for different levels of deformation (hardening interphase case; simple tensile loading; aluminium adherends).

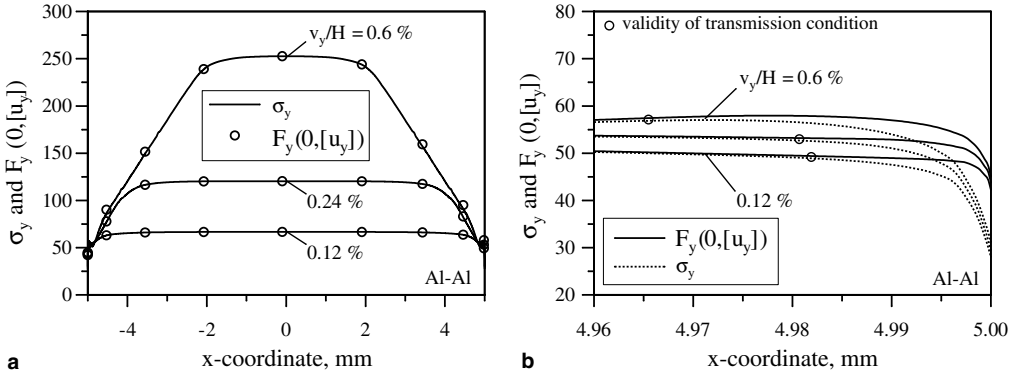

Fig. 8. Determination of the validity of the transmission condition for an elasto-plastic interphase (hardening interphase case; simple tensile loading; aluminium adherends).

chosen to indicate the validity regions for the transmission conditions. The regions are of 2–3 thickness of the interphase. It is also important to note that the plastic zones appearing near the free edges are very small and are invisible in the scale of Fig. 8(a). The zone where the transmission conditions are not longer valid coincides more or less with the range of the singularity dominated domains for the elastic interface [12] and becomes to be smaller with accumulated plastic deformation.

3.1.1.2. Combined loading. Now we apply to the top of the specimen a combined loading in such a way that in y-direction the same displacement is prescribed whereas in the perpendicular direction there is also a non-zero monotonic loading: $(u_x(x, H/2) = v_x, u_y(x, H/2) = v_y)$ in the same ranges from 0% to 0.6% for v_y/H and v_x/H, respectively, in 100 incremental steps.

In this case, the same particularities can be observed with respect to distributions of the displacements and stresses inside the thin interphase and outside the interphase within the surrounding materials. In Fig. 9, the results concerning Huber–Mises stress and equivalent plastic strain are presented in the same way as it has been done in Fig. 7. A slightly different behaviour can be observed which shows now the influence of the additional secondary loading in x-direction.

A more interesting question is about the validity of the transmission conditions. Now both of them are not trivial. Moreover, a second non-zero jump $[u_x]$ is presented in the functions F_x, F_y appearing in the transmission conditions (17). It is interesting to note that the validity region is at least not smaller than in the case of the simple tensile loading. To manifest this, we present Fig. 10 where the same values are depicted as in Fig. 8.

The same accuracy for the evaluated transmission conditions arises for the second transmission condition dealing with the jump $[u_x]$. We skip this picture only because it cannot be compared with the case of the simple tensile loading.

One of the crucial points to underline is the fact that the stress-strain state of the 2D bimaterial structure under consideration is not pure monotonic due to the definition in [15]. Thus, it would be natural to expect a more essential difference between the numerical model based on the plastic flow theory and the analytically predicted interfacial conditions based on the deformation theory in comparison with the accuracy observed for the pure elastic interface. However, as it follows from the results presented in Figs. 8 and 10, the accuracy of the transmission conditions is

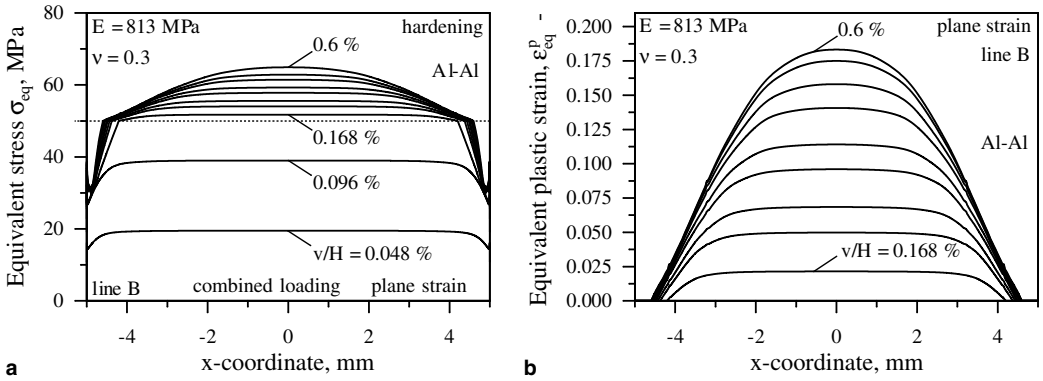

Fig. 9. Distribution of equivalent stress and strain along line B (cf. Fig. 1) for different levels of deformation (hardening interphase case; combined loading; aluminium adherends).

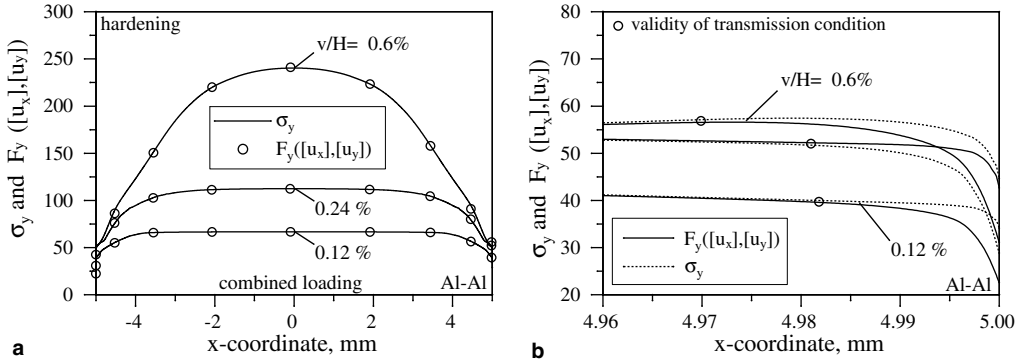

Fig. 10. Determination of the validity of the transmission condition for an elasto-plastic interphase (hardening interphase case; combined loading; aluminium adherends).

much better than one can even expect due to the limitation of the deformation theory. However, this is only true for a hardening interphase law. It will be shown in the following that the results are slightly worse in the case of perfect plasticity. It should be noted here that the adherends remained in the pure elastic regime at any stage of the applied deformation.

3.1.2. Elasto-plastic interphase with perfect plasticity

3.1.2.1. Simple tensile loading. In this case, also the same monotonic tensile loading $(u_x(x, H/2) = 0, u_y(x, H/2) = v_y)$ has been applied to the top of the bimaterial sample in range from 0% to 0.4% of v_y/H in 200 incremental steps. Because of the perfect plasticity law in the plastic region, one should increase the accuracy of the calculations.

The results concerning the behaviour of the solution within the interphase in direction perpendicular to the glue line ($y = 0$) are similar to those shown in Figs. 5 and 6 at point $x = 0$ and hold without any conceptual change (constant stresses and linear displacements at each increment). Distributions of the equivalent Huber–Mises stress and the equivalent plastic strain along the middle line of the elasto-plastic interphase ($y = 0$) are presented for several increments in Fig. 11. One can clearly observe the ideal plasticity plateau starting from a total deformation of $v_y/H = 0.14\%$.

The verification of the transmission condition $(8)_2$ in this case is presented in Fig. 12. Still very good agreement with the theoretical results can be observed over the whole range of the interface.

3.1.2.2. Combined loading. Let us now consider a combined loading. In this case it will be a monotonically increasing external loading $(u_x(x, H/2) = v_x, u_y(x, H/2) = v_y)$ applied to the top of the bimaterial sample in the same range from 0% to 0.4% for v_y/H and v_x/H, respectively, in 200 incremental steps.

We also restrict ourselves to show the same results as for the simple tensile loading case. Respective equivalent Huber–Mises stress and equivalent plastic strain curves are presented in Fig. 13, whereas the verification of the validity of the transmission conditions can be done based in Fig. 14.

A very important difference in comparison with the hardening law can be observed in the case of the ideal plasticity law. Namely, the region where the transmission conditions are valid is smaller than that in the case of the hardening plastic law (compare Figs. 8(b) and 10(b)) and this region essentially depends on the level of plastic deformation (compare Figs. 12(b) and 14(b)). To clarify the difference, some estimates of the zone ends have been presented in Table 1 for the hardening and the ideal plasticity law for different levels of the deformation. However, in

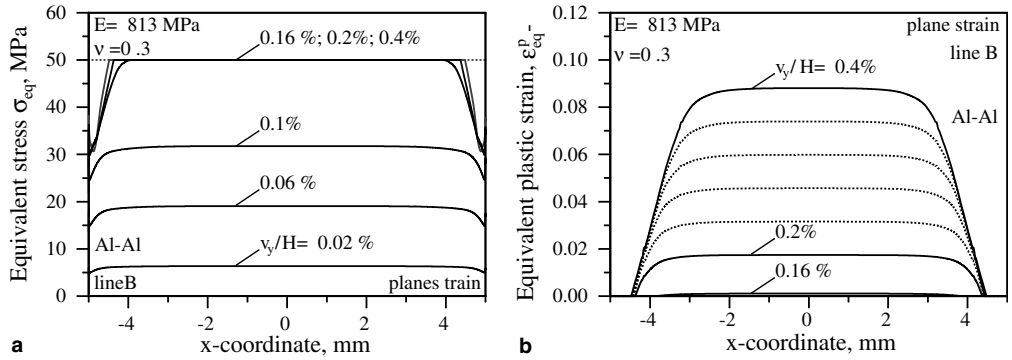

Fig. 11. Distribution of equivalent stress and strain along line B (cf. Fig. 1) for different levels of deformation (ideal plasticity interphase; simple tensile loading; aluminium adherends).

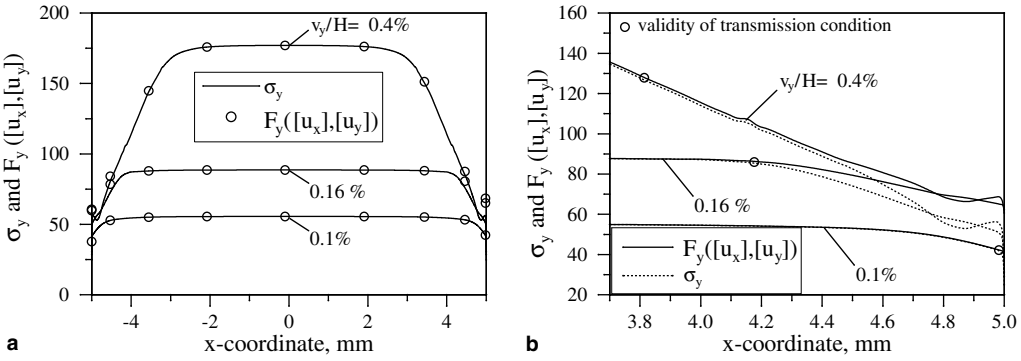

Fig. 12. Determination of the validity of the transmission condition for an elasto-plastic interphase (ideal plasticity interphase; simple tensile loading; aluminium adherends).

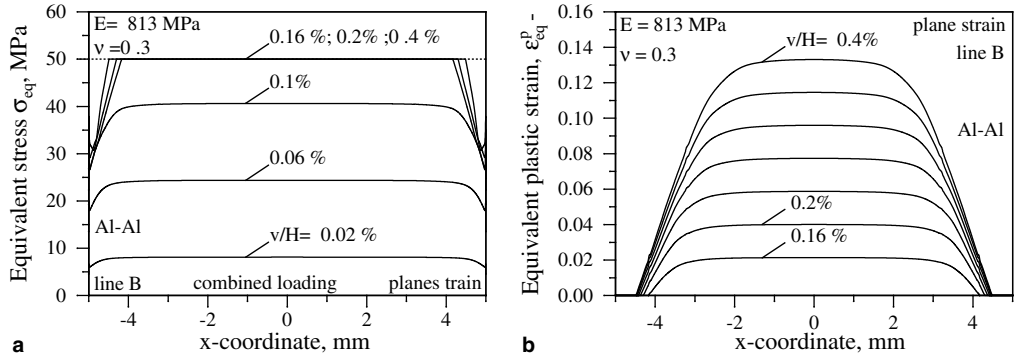

Fig. 13. Distribution of equivalent stress and strain along line B (cf. Fig. 1) for different levels of deformation (ideal plasticity interphase; combined loading; aluminium adherends).

both cases application of combined loading provided slightly better results for the applicability of the transmission conditions. This is an important result. First of all because a combined external loading is more frequent in technical applications. On the other hand, it shows that the worse accuracy appears in simple loading cases which researchers usually apply for testing.

3.2. Fibre reinforced plastics

All previous simulations and evaluations were performed for adhesively bonded metallic joints made of aluminium adherends. In the following sections, typical material parameter sets taken from the context of fibre-reinforced plastics (FRP) were assigned to the same finite element model as described in Section 3.1. For simplicity, the fibres were assumed to reveal an isotropic, homogeneous and linear-elastic behaviour and possible effects resulting from curvatures were neglected in order to compare the results with findings obtained in the previous section. For both types of fibres, i.e. glass and carbon, the interphase consists of the same elasto-plastic epoxy matrix with elastic constants $E = 3000$ MPa and $v = 0.4$ [20]. The plastic parameters of the interphase, i.e. initial yield stress $k_{t,0} = 45$ MPa and

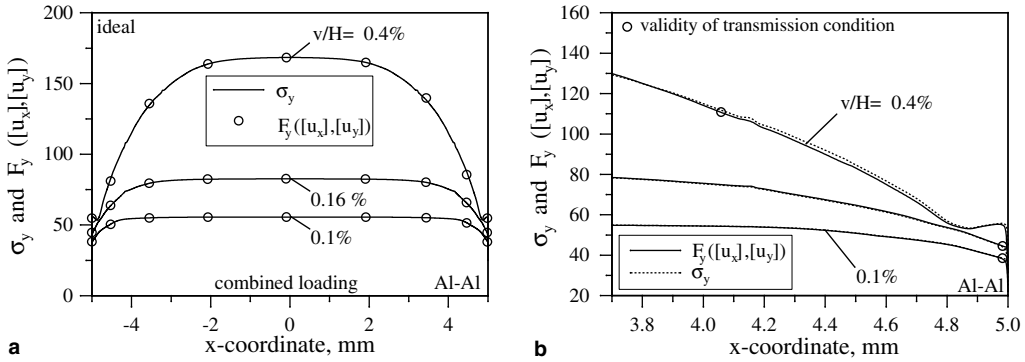

Fig. 14. Determination of the validity of the transmission condition for an elasto-plastic interphase (ideal plasticity interphase; combined loading; aluminium adherends).

Table 1
Validity of the transmission condition in terms of $\delta/(2h)$ for metallic joints

	Deformation	0.12%	0.22%	0.6%
Hardening				
	Simple tensile	1.81	1.93	3.45
	Combined loading	1.82	1.90	3.01
Ideal		0.1%	0.16%	0.4%
	Simple tensile	1.78	82.35	118.6
	Combined loading	1.82	1.80	94.2

linear hardening modulus $E_p = 2200$ MPa were taken from Ref. [21], cf. graphical representation given in Fig. 15a).

The respective function ϕ involved in the deformation theory Eqs. (1) and (2) has been calculated by the given interphase properties of the flow theory [15,16] and its graph is shown in Fig. 15(b). Furthermore, it was assumed that the elasto-plastic matrix is obeying the Huber–Mises yield criterion.

3.2.1. Glass fibres and epoxy matrix

In the following section, a typical material set for glass fibres, i.e. $E_{\pm} = 66{,}500$ MPa and $v_{\pm} = 0.23$ [22], is considered. The same external monotonic tensile loading as in the case of metallic joints ($v_y/H = 0.006$) is applied in 100 incremental steps. Fig. 16 shows the distribution of equivalent Huber–Mises stress and strain along the middle line ($y = 0$) of the elasto-plastic interphase for different levels of deformation. Comparing this figure with the results obtained in the previous section (cf. Fig. 7), one can observe that the behaviour is quite different. Namely, a practical constant behaviour for both quantities is obtained over a wide range of the interphase for the fibre–matrix structure. In addition to that, small maxima occur now close to the free surface while the material set for the metallic structure reveals its maximum in the middle where $x = y = 0$ holds.

Comparing the results for the equivalent plastic strains (i.e. Figs. 16(b) and 7(b)), one can see that the level for the plastic strain is much lower in the case of the fibre–matrix material set which is a direct result of the chosen material parameters. Despite the lower initial yield stress, first plastic deformation occurs a few increments later in the case of the fibre–matrix material because the equivalent yield stress is much more homogeneously distributed over the length of the interphase.

The validity of the transmission condition is shown in Fig. 17. As can be seen, a perfect fulfilment is again obtained over the range presented in Fig. 17(a). Looking at the magnification shown in Fig. 17(b), one can observe that the range of the validity decreases from $x \approx 4.9$ (cf. Fig. 8(b)) to $x \approx 4.5$ compared to the metallic configuration. This is an important information in order to decide

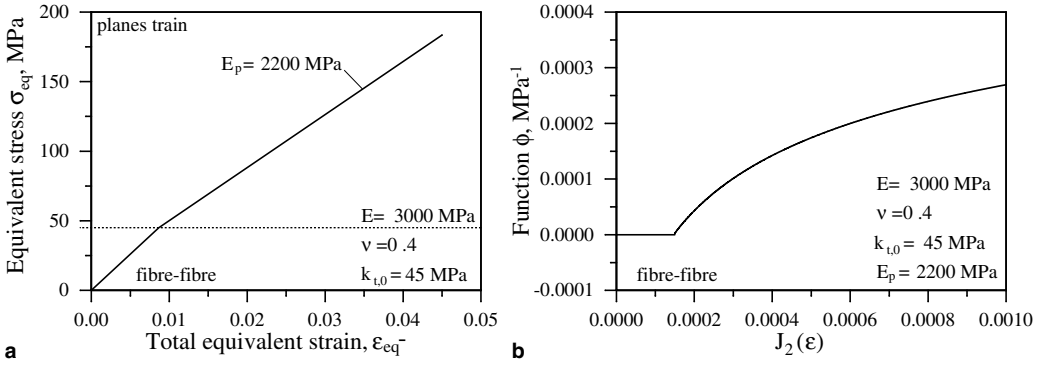

Fig. 15. (a) Material parameters of the interphase for fibre reinforced plastics due to plastic flow theory and (b) function ϕ of Hencky's law.

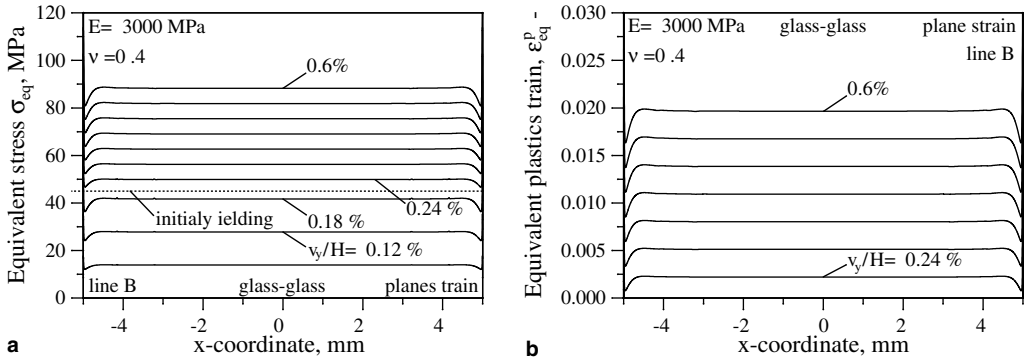

Fig. 16. Distribution of equivalent stress and strain along line B (cf. Fig. 1) for different levels of deformation (hardening interphase case; simple tensile loading; glass adherends).

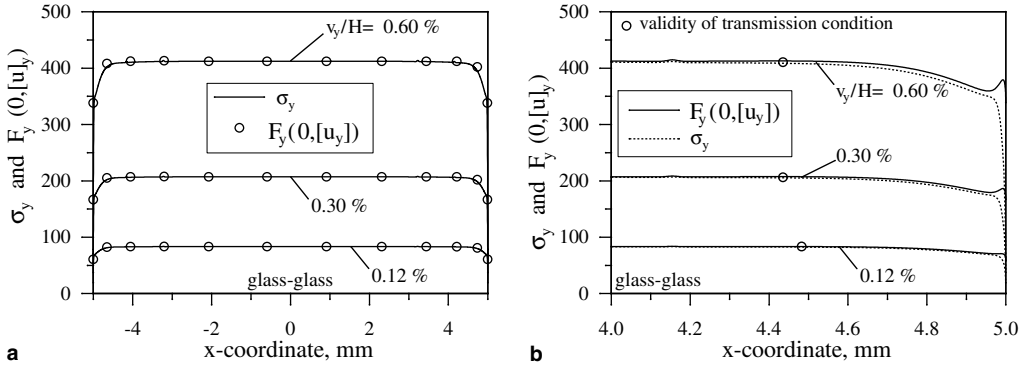

Fig. 17. Determination of the validity of the transmission condition for an elasto-plastic interphase (hardening interphase case; simple tensile loading; glass adherends).

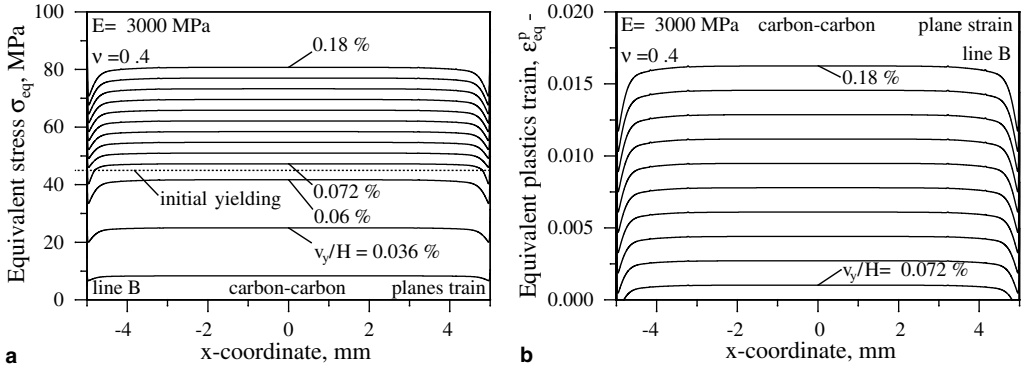

Fig. 18. Distribution of equivalent stress and strain along line B (cf. Fig. 1) for different levels of deformation (hardening interphase case; simple tensile loading; carbon adherends).

where interphase or special singularity elements should be introduced in an improved numerical approach. Nevertheless, a range of $x \approx 4.5$ for the validity is from a practical point of view still quite good.

3.2.2. Carbon fibres and epoxy matrix

A typical set for carbon fibres ($E_{\pm} = 227{,}000$ MPa and $v_{\pm} = 0.3$ [20]) is assigned for the adherends in the following section. In order to obtain comparable values for the equivalent plastic strain, the maximum evaluated external displacement is limited to $v_y/H = 0.0018$. As in the previous example of a fibre reinforced plastic, a homogeneously distribution of the equivalent stress and strain is obtained, cf. Fig. 18.

Looking at Fig. 19 which illustrates the validity of the transmission condition, one can see that a validity region ($x \approx 4.95$) is significantly larger than in the case of the glass–fibre material set and now comparable to the values

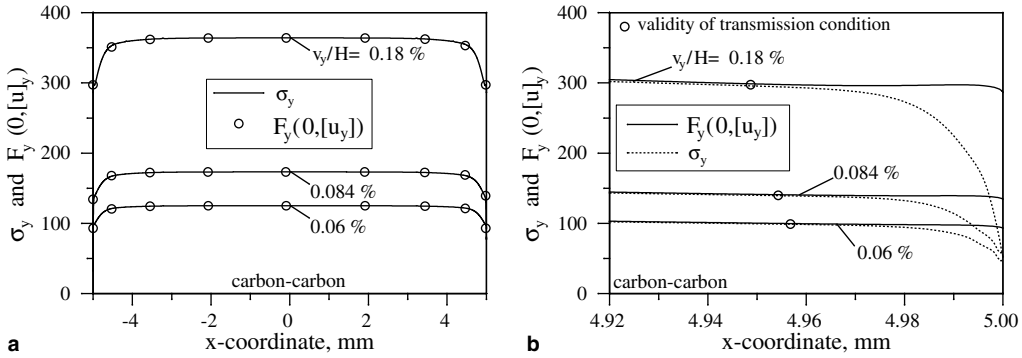

Fig. 19. Determination of the validity of the transmission condition for an elasto-plastic interphase (hardening interphase case; simple tensile loading; carbon adherends).

Table 2
Validity of the transmission condition in terms of $\delta/(2h)$ for fibre reinforced plastics (hardening)

Material	Deformation	0.12%	0.30%	0.6%
Glass–glass	Simple tensile	51.74	56.42	56.55
	Deformation	0.06%	0.084%	0.18%
Carbon–carbon	Simple tensile	4.32	4.57	5.13

obtained for the metallic joint. It should be noted here that the same range compared to the metallic joints could be obtained even though the material properties for the interphase and the level of the external loading are quite different.

The normalised values for the validity of the transmission conditions for fibre–matrix material sets are summarised in Table 2. As can be seen, the much stiffer carbon fibre reveals results comparable to the metallic joint set and significantly better than the glass fibre. Reminding that the interphase material was the same for both fibre–matrix cases, one can see that the stiffness ratio between interphase and joint materials directly influences the validity of the transmission conditions.

4. Discussions and conclusion

The very good accuracy of the presented approach will enable the introduction of novel finite elements for thin interphases. Later, we concentrate on the weak side of the method and its respective restrictions.

It follows from Eqs. (6) and (11) that $\nu \leqslant \tilde{\nu}(\phi) \leqslant 1/2$ and $\tilde{\nu}(\phi) \to 1/2$ for $\phi \to \infty$. Hence, it may happen for large plastic deformations that the generalised Poisson's ratio will approaches its maximal value of 0.5 and, as a result, the transmission conditions evaluated here should be used with a reservation as it follows from the results obtained in [23] for the weakly compressible soft elastic interface. Nevertheless, if Poisson's ratio of the elasto-plastic interphase is sufficiently smaller than 0.5 in the elastic regime, then in the range of usual plastic deformations, the transmission conditions which were evaluated in the paper can be applied.

For example, the maximum value of the generalised Poisson's coefficient (6) in the numerical simulation for the 100th increment with a deformation ratio of $v_y/H = 0.6\%$ (hardening case) takes the value $\tilde{\nu} = 0.47$, while $\tilde{\nu}(0) = 0.3$. Additionally, values of the generalised Poisson's ratio are presented in Fig. 20 for four different adhesive materials. Three of them (hardening law and ideal plasticity law for the interphase in metallic joints and fibre reinforced plastics) were used earlier in this paper and the last one is from Ref. [24] where properties of real adhesive have been discussed. One can conclude from Fig. 20 that the ideal plasticity case is the most dangerous in the discussed sense. Also it provides the worst results with respect to the validity of the transmission conditions (16) and (17), cf. Tables 1 and 2.

The transmission conditions (16) and (17) which were evaluated in the paper are non-linear and the jumps of the displacements in different directions with respect to the bimaterial interface cannot, generally speaking, be separated from each other. This only occurs in the elastic regime. Another possibility where the jumps are separated, even under plastic regime, appears in the case of some special loadings (simple tension or simple shear), where one of the non-linear transmission conditions (17) is satisfied identically whereas the other contains on the left-hand side the

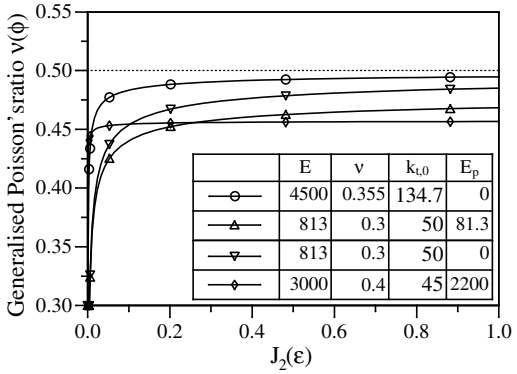

Fig. 20. Generalised Poisson's ratio (cf. Eq. (6)) for different adhesive materials.

only remaining non-zero jump (generally speaking in the non-linear form).

Additionally, to the presented analysis, investigations of the possible singularity of the solution for a bimaterial body with the soft imperfect elasto-plastic interface model near the interface crack tip or near free edge should be done. Respective results concerning pure elastic imperfect interface have been obtained in [8–10].

Acknowledgements

This work was established during a short visit of G. Mishuris at the University of Aveiro supported by the Centre for Mechanical Technology and Automation and has been completed as a part of his research activity as Marie Curie Fellow at University of Liverpool in ToK scheme with the grant MTKD-CT-2004-509809. A. Öchsner is grateful to Portuguese Foundation of Science and Technology for financial support.

Appendix

Here, only the main ideas in a comprehensive form how to evaluate transmission conditions (16) and (17) are presented. For more details and proof, a prospective reader is requested to the paper [18].

Let us consider a bi-material domain with a thin elasto-plastic layer between two different elastic materials (Fig. 1) which can be described by Hencky's law (1) in such a way that the conditions

$$2h = 2\epsilon h_0, \quad \tilde{\mu} = \epsilon\tilde{\mu}_0, \quad \tilde{\lambda} = \epsilon\tilde{\lambda}_0, \tag{9}$$

are simultaneously satisfied with some small parameter $\epsilon \ll 1$, and

$$h_0 \sim L, \quad \tilde{\mu}_0 \sim \mu_{\pm}, \quad \tilde{\lambda}_0 \sim \lambda_{\pm}, \tag{10}$$

while L is a characteristic size of the body and $\mu_{\pm}$, $\lambda_{\pm}$ are the respective generalised Lamé's coefficients of the adherends which are much higher under the same level of deformation than the corresponding values of the elasto-plastic interface. Let us note that it is sufficient to use instead of $\tilde{\mu}$ and $\tilde{\lambda}$ in estimate (9) its value in the elastic region because

$$0 < \tilde{\mu}(\phi) \leqslant \mu, \quad \lambda \leqslant \tilde{\lambda}(\phi) < \frac{1+\nu}{3\nu}\lambda \tag{11}$$

and Poisson's ratio of the interphase is rather different from zero. Moreover, one can show [18] that the function $\tilde{\mu}(\phi)$ monotonically decreases, while functions $\tilde{\nu}(\phi)$ and $\tilde{\lambda}(\phi)$ monotonically increase.

Within the interface together with Eq. (1), the equilibrium equations should be satisfied:

$$\frac{\partial\sigma_x}{\partial x} + \frac{\partial\sigma_{xy}}{\partial y} = 0, \quad \frac{\partial\sigma_{xy}}{\partial x} + \frac{\partial\sigma_y}{\partial y} = 0, \quad y \in (-\epsilon h_0, \epsilon h_0). \tag{12}$$

Along the two bimaterial interfaces between the layer and the adherends ($y = \pm\epsilon h_0$), the perfect transmission conditions are assumed to be along the interphase boundaries true:

$$u_x(x, \pm\epsilon h_0) = u_x^{\pm}(x, \pm\epsilon h_0), \quad u_y(x, \pm\epsilon h_0) = u_y^{\pm}(x, \pm\epsilon h_0), \tag{13}$$

$$\sigma_{xy}(x, \pm\epsilon h_0) = \sigma_{xy}^{\pm}(x, \pm\epsilon h_0), \quad \sigma_y(x, \pm\epsilon h_0) = \sigma_y^{\pm}(x, \pm\epsilon h_0). \tag{14}$$

Following for [25], we search for a possible solution in a form of asymptotic series:

$$\mathbf{u}(x,y) = \sum_{j=0}^{\infty} \epsilon^j \mathbf{u}_j(x,\xi), \quad \boldsymbol{\sigma}(x,\xi) = \sum_{j=0}^{\infty} \epsilon^j \boldsymbol{\sigma}_j(x,\xi). \tag{15}$$

To construct the asymptotic procedure [25], it is necessary to collect in all equations and in the transmission conditions the terms of the same order with respect to the small parameter ε and then to solve step by step the corresponding boundary value problems. Thus, repeating the line of the reasoning as in [11] one can find the solution for the zero-order approximation within the interface in the following form [18]:

$$[\sigma_{xy}]_{y=0} = 0, \quad [\sigma_y]_{y=0} = 0, \tag{16}$$

$$F_x([u_x],[u_y]) = \sigma_{xy}, \quad F_y([u_x],[u_y]) = \sigma_y, \tag{17}$$

$$F_x = \frac{1}{2h}\tilde{\mu}(\phi(J_2(\boldsymbol{\varepsilon}))) \cdot [u_x],$$

$$F_y = \frac{1}{2h}(\tilde{\lambda} + 2\tilde{\mu})(\phi(J_2(\boldsymbol{\varepsilon}))) \cdot [u_y]. \tag{18}$$

It was proven in [18] that all values within the interphase do not depend on the variable y in the main terms, such that $J_2(\boldsymbol{\varepsilon}) = J_2(x)$, $\phi(J_2(\boldsymbol{\varepsilon})) = \phi(x)$, and

$$J_2(\boldsymbol{\varepsilon}) = \frac{[u_x]^2}{16h^2} + \frac{[u_y]^2}{12h^2}. \tag{19}$$

Note here that functions $F_x(t,\cdot)$ and $F_y(\cdot,t)$ in (17) monotonically increase with respect to the variable t.

Eqs. (16) and (17) substitute the complete system of non-linear transmission conditions for the soft elasto-plastic interface in a bimaterial structure.

References

[1] Benveniste Y. The effective mechanical behaviour of composite materials with imperfect contact between the constituents. Mech Mater 1985;4:197–208.

[2] Erdogan F. Fracture mechanics of interfaces. In: Proceedings of the first international conference on damage and failure of interfaces DFI-I/Vienna/22–24 September 1997, Rotterdam-Brookfield. p. 3–36.

[3] Hashin Z. Thermoeleastic properties of fiber composites with imperfect interface. Mech Mater 1990;8:3333–48.

[4] Avila-Pozos O, Klabring A, Movchan AB. Asymptotic model of orthotropic highly inhomogeneous layered structure. Mech Mater 1999;31:101–15.

[5] Benveniste Y, Miloh T. Imperfect soft and stiff interfaces in two-dimensional elasticity. Mech Mater 2001;33:309–23.

[6] Hashin Z. Thin interphase/imperfect interface in elasticity with application to coated fiber composites. J Mech Phys Solids 2002;50:2509–37.

[7] Klabring A, Movchan AB. Asymptotic modelling of adhesive joints. Mech Mater 1998;28:137–45.
[8] Antipov YA, Avila-Pozos O, Kolaczkowski ST, Movchan AB. Mathematical model of delamination cracks on imperfect interfaces. Int J Solids Struct 2001;38:6665–97.
[9] Mishuris G. Interface crack and nonideal interface approach. Mode III. Int J Fract 2001;107(3):279–96.
[10] Mishuris G, Kuhn G. Asymptotic behaviour of the elastic solution near the tip of a crack situated at a nonideal interface. ZAMM 2001;81(12):811–26.
[11] Mishuris G, Öchsner A, Kuhn G. Imperfect interfaces in dissimilar elastic body: FEM-analysis. In: Ren Z, Kuhn G, Skerget L, Hribersek M, editors. Advanced Computational Engineering Mechanics. Proc. of the First Workshop, Maribor Slovenia, October 9–11, 2003. Maribor: University of Maribor Publishers; 2003. p. 101–10.
[12] Mishuris G, Öchsner A. Edge effects connected with thin interphases in composite materials. Compos Struct 2005;68:409–17.
[13] Rosselli F, Carbutt P. Structural bonding applications for the transportation industry. Sampe J 2001;37(6):7–13.
[14] Ikeda T, Yamashita A, Lee D, Miyazaki N. Failure of a ductile adhesive layer constrained by hard adherends. Trans ASME J Engng Mater Technol 2000;122:80–5.
[15] Kachanov LM. Fundamentals of the theory of plasticity. Moscow: MIR Publishers; 1974.
[16] Chen WF. Constitutive equations for engineering materials. Amsterdam: Elsevier; 1994.
[17] Hill R. The mathematical theory of plasticity. Oxford: Clarendon Press; 1998.
[18] Mishuris G, Öchsner A. Transmission conditions for a soft elasto-plastic interphase between two elastic materials. Plane strain state. Arch Mech 2005;57(2–3):157–69.
[19] Öchsner A, Winter W, Kuhn G. Damage and fracture of perforated aluminum alloys. Adv Eng Mater 2000;2(7):423–6.
[20] Blassiau S, Thionnet A, Bunsell AR. Micromechanisms of load transfer in a unidirectional carbon fibre-reinforced epoxy composite due to fibre failures. Part 1: Micromechanisms and 3D analysis of load transfer: the elastic case. Compos Struct 2006;74(3):303–18.
[21] Blassiau S, Thionnet A, Bunsell AR. Micromechanisms of load transfer in a unidirectional carbon fibre-reinforced epoxy composite due to fibre failures. Part 2: Influence of viscoelastic and plastic matrices on the mechanisms of load transfer. Compos Struct 2006;73(3):319–31.
[22] Palacz M, Krawczuk M, Ostachowicz W. The spectral finite element model for analysis of flexural-shear coupled wave propagation. Part 1: Laminated multilayer composite beam. Compos Struct 2005;68:37–44.
[23] Mishuris G. Imperfect transmission conditions for a thin weakly compressible interface. 2D Problems. Arch Mech 2004;56(2):103–15.
[24] Jeandrau JP. Analysis and design data for adhesively bonded joints. Int J Adhes Adhes 1991;11(2):71–9.
[25] Movchan AB, Movhan NV. Mathematical modelling of solids of with nonregular boundaries. Boca Raton: CRC Press; 1995.